Volume 7, Number 2, 2014. pp. 53-63

Jordan Journal of Physics

ARTICLE

One-Step Synthesis of Fe-Doped ZnO Thin Films by a Convenient Electrochemical Technique at Room Temperature

M. A. Awawdeh[a], **K. Al-Heuseen**[b] **and I. M. Odeh**[a]

[a] *Department of Physics, Yarmouk University, Irbid, Jordan.*
[b] *Ajloun University College, Al-Balqa Applied University, Ajloun, Jordan.*

Received on: 9/9/2013; Accepted on: 18/5/2014

Abstract: This paper reports on the synthesis and characterization of Fe-doped ZnO thin films deposited onto gold coated glass substrates, using electrochemical deposition (ECD) technique at room temperature and different concentrations of Fe. X-ray diffraction (XRD), scanning electron microscopy (SEM), photoluminescence (PL) and optical transmission measurements were used to characterize the films. The effect of iron doping on the structural, morphological and optical properties of the films was studied. The XRD spectra of the Fe-ZnO films indicate the polycrystalline nature having hexagonal crystal structure. From the XRD pattern, it is observed that peak positions shift toward lower angles with Fe doping. The change in the peak positions with increase in Fe content clearly indicates that Fe ions replace Zn ions in the ZnO films. The SEM images showed different surface morphologies of the grown structures on the gold layer according to the doping concentration. The shape and dimensions of the structures depend on the doping level. The PL spectra illustrate that there is an obvious red-shift for the emission centre from ultraviolet to blue region. The intensities of emissions from defects increase with the increase of Fe doping. The growth and doping mechanism was also briefly discussed.

Keywords: Fe-doped ZnO thin films; Nanomaterials; Doping; Electrochemical deposition; ZnO.

Introduction

Transparent metal oxide films are of paramount technological importance for solar cells, chemical sensors, liquid crystal displays and as nano porous films for dye sensitized solar cells. Among these metal oxides, wide direct band-gap zinc oxide (ZnO) has gained increasing attention because of its promising properties. ZnO has a broad range of applications, such as light-emitting diodes, photo detectors and gas sensors [1-4]. The interest in ZnO is due to its unique properties, such as a relatively high exciton binding energy (60 MeV), wide band gap (3.34 eV at 300 K), piezoelectric behavior and the fact that it is a biocompatible material.

The undoped/doped ZnO can be fabricated using various methods, such as radio frequency plasma [5], ion-assisted cyclic sputtering [6], RF sputtering [7], thermal oxidation [8], electron beam evaporation [9], activated reactive evaporation [10], spray pyrolysis [11], low-pressure metal organic chemical vapor deposition (MOCVD) [12], chemical bath deposition [13] and electrodeposition [14].

Compared to other techniques, electrochemical methods offer several advantages including fast, simple, low cost operation at near room temperature, large-scale deposition area and the ability to control composition, crystallinity and the properties of the deposit by adjusting deposition conditions. It is interesting that the electrodeposition of ZnO can also produce a variety of different morphological deposits [15]. In addition, the

Corresponding Author: M. A. Awawdeh **Email**: amufeed@yu.edu.jo.

preparation of ZnO by electrodeposition is also eco-friendly because normally no toxic chemicals are used in the electrolytic bath [15-17]. Moreover, the deposition process can be carried out on various substrates such as glass, polymers, semiconductors and templates. There are no special requirements needed for the substrates, except that they should be conductive. Therefore, this technique is well adapted for industrial procedures in the fabrication of ZnO thin films.

Furthermore, ZnO thin films are also considered as a host material for diluted magnetic semiconductors (DMS) by transition metal elements doping [18-21]. The possibility of synthesizing ferromagnetic ZnO nanostructures is particularly encouraging, since this will enable several promising applications in the fields of spintronics and optoelectronics.

However, several inconsistent results have been obtained for the Fe-doped ZnO films. Polyakov et al. [22] found room temperature ferromagnetism by implanting Fe ions in a ZnO crystal grown by vapour phase, while Janisch et al. [23] reported that Fe-doped ZnO showed a paramagnetic behavior. In order to clarify this discrepancy, it is important to disclose the effect of doped-Fe on the structure and properties of ZnO thin films. For the Fe-doped ZnO materials, the results of some theoretical studies show that they can possess ferromagnetic properties at room temperature [24, 25]; therefore, most of the researchers mainly studied the ferromagnetic behavior of Fe-doped ZnO thin films [26-28]. There are few reports on their structural, optical and electrical properties. However, Fe-doped ZnO thin film could be an important multi-functional material; hence, it is important to study its structural, optical and electrical properties and the correlation between them.

In this work, we prepared Fe-doped ZnO nanostructures at room temperature by electrochemical techniques on gold coated glass substrates in an aqueous solution. The novelty of synthesis of thin films at room temperature is to reduce the thermal mismatch between films and substrates. The effect of Fe-doping concentration on the structural and optical properties of ZnO nanostructure was investigated. Structural and optical properties were investigated by scanning electron microscopy (SEM), X-ray diffraction (XRD) and photoluminescence (PL) spectroscopy.

Experimental Procedure

Fe doped ZnO nanostructures were deposited by electrochemical deposition (ECD) using 0.1 M Zn $(NO_3)_2$ aqueous solutions and a stock solution of 4.13 mM Fe $(NO_3)_3$ dissolved in deionized water. To adjust the composition of the deposits, the concentrations of Fe $(NO_3)_3$ in the baths were 10 µl, 20 µl, 30 µl and 40 µl. These correspond to the concentrations of Fe ions in the bath of 0.06 mM, 0.12 mM, 0.18 mM and 0.24 mM, respectively.

A simple two-electrode homemade Teflon cell was constructed using a platinum wire as an anode and the gold coated glass substrate as a cathode. The gold coating is sufficiently thin such that it allows transmittance measurements unhindered. The thicknesses of gold layers were about 20 nm. The distance between the anode and the substrate was about 5 mm. A constant electrodeposition current density of 3 mA/cm^2 producing the highest deposition rate was applied for 30 min. The good conducting gold layer was used to reduce the stress in the deposited films and to increase the deposition rate.

The possible electro-deposition mechanism of ZnO through nitrate precursors can be summarized as follows:

First, the reduction of nitrate ions produces nitrite and hydroxide ions in water. Then, Zn ions interact with hydroxide ions, forming Zinc Hydroxides. After dehydration of Zn $(NO_3)_2$, the final product ZnO forms [29].

$$Zn(NO_3)_2 + H_2O \rightarrow Zn^{2+} + NO_3^{1-} \quad (1)$$

$$NO_3^{1-} + H_2O + 2e^- \rightarrow NO_2^{1-} + 2OH^- \quad (2)$$

$$Zn^{2+} + 2OH^{1-} \rightarrow Zn(OH)_2 \quad (3)$$

$$Zn(OH)_2 \rightarrow ZnO + H_2O \quad (4)$$

Since iron oxides thin films were electrodeposited in an aerated solution, there are two possible reactions to accomplish the formation of Fe_2O_3.

Reaction 1

Dissolved oxygen can be reduced and then react with ferric ions to form Fe_2O_3 as in the following reaction:

$$4Fe^{3+} + 3O_2 + 12e^- \rightarrow 2Fe_2O_3 \quad (5)$$

This reaction is limited by the concentration of the dissolved oxygen.

Another possible reaction is manifested *via* water dissociation as shown in Eq. (6a). This enhances the formation of ferric hydroxide as in Eq. (6b). Ferric hydroxide is converted into Fe_2O_3 as in Eq. (6c). The overall reaction is shown in Eq. (6d). Due to the low dissolved oxygen concentration in the reaction cell, this suggests that reaction 2 is the predominant electrodeposition reaction pathway [30].

Reaction 2

$$6H_2O + 6e^- \rightarrow 3H_2\,(g) + 6OH^- \qquad (6a)$$

$$2Fe^{3+} + 6OH^- \rightarrow 2\,Fe(OH)_3 \qquad (6b)$$

$$2\,Fe(OH)_3 \rightarrow Fe_2O_3 + 3H_2O \qquad (6c)$$

$$2Fe^{3+} + 6H_2O + 6e^- \rightarrow Fe_2O_3 + 3H_2\,(g) \qquad (6d)$$

Finally, the synthesized products were characterized by X-ray diffraction (XRD), scanning electron microscopy (SEM) and photoluminescence (PL) spectroscopy.

High resolution XRD (PANalytical X'pert Pro MRD) with a Cu-Kα_1 radiation source (λ = 1.5406 Å) is used to assess the crystalline quality and the lattice parameters of the samples which can also be determined from the peak position. Under high resolution measurements, this system has a resolution of 12 arcsec. The grain structure and stoichiometry of the prepared samples were examined by scanning electron microscope (SEM FEI Quanta 200) equipped with energy dispersive X-ray spectroscopy (EDAX) facility for elemental analysis.

For SEM characterization, normally the measurements were performed at 10 kV to measure the surface morphology of the samples.

Photoluminescence (PL) measurements were performed by using Jobin Yvon HR800UV spectrometer system that is an integrated confocal micro-photoluminescence spectrometer. A helium cadmium (He-Cd) laser (325 nm) and an argon ion laser (514.5 nm) were used as excitation sources for PL measurements; the incident laser power was 20 mW.

Results and Discussion

Fig.1 (A) shows XRD spectra of (a) pure ZnO, (b) 0.06 mM Fe, (c) 0.12 mM Fe, (d) 0.18 mM Fe and (e) 0.24 mM Fe-doped ZnO thin films, respectively. In all cases, the observed diffraction peaks can be indexed to standard hexagonal wurtzite ZnO structure, indicating that Fe-doping did not change the hexagonal wurtzite structure of ZnO films. Seven peaks appear in the diffraction spectrum in the 2θ interval of 30-70° and correspond to (100), (002), (101), (102), (110), (103) and (112) orientations of the ZnO hexagonal structure. The film formed is polycrystalline with a preferential orientation of the (002) diffraction peak, showing that the film is preferentially oriented along the c-axis direction. This indicates that this axis in the ZnO film tends to grow perpendicular to the substrate surface [31]. In the XRD pattern, characteristic peaks of the (111) gold substrate also appears.

Fig. 1B shows the main characteristic peaks ((100), (002), (101)) of wurtzite structure in order to see a close view and the impact of the dopant ions in the pristine ZnO lattice. The peaks are shifted to lower angles and the intensity decreased with increasing Fe doping concentration compared to those of pure bulk ZnO, which is consistent with that of other Fe-doped ZnO films [31]. This shift in peak positions clearly reflects that Fe replaces Zn in the ZnO films. Meanwhile, it was apparent that the intensity and the full width at half maximum (FWHM) of (002) diffraction peak decreases with the increment of Fe concentration, implying that more Fe concentration in ZnO films improves the ZnO film crystallinity.

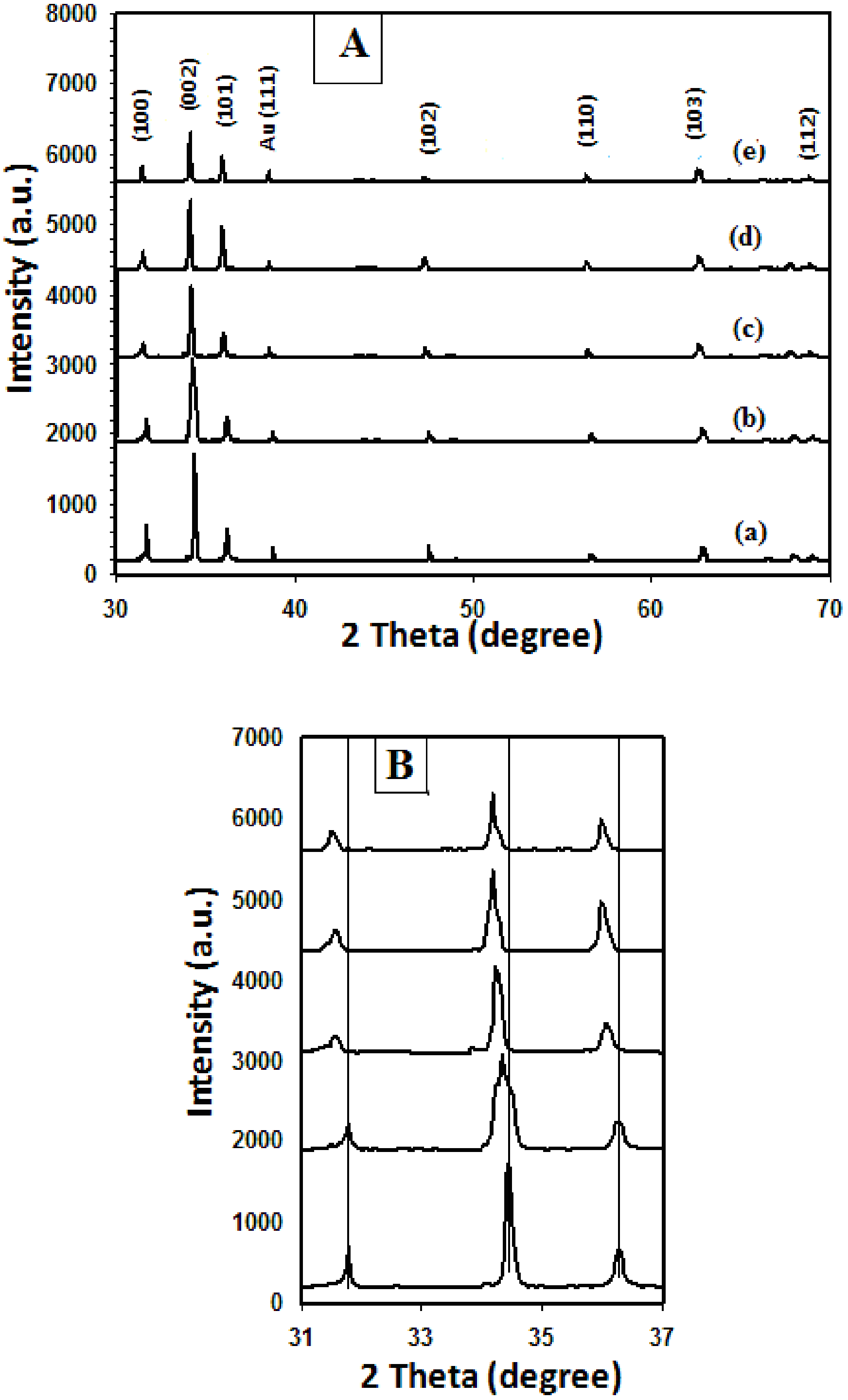

FIG. 1. (A) XRD spectra of of (a) pure ZnO, (b) 0.06 mM Fe, (c) 0.12 mM Fe, (d) 0.18 mM Fe and (e) 0.24 mM Fe-doped ZnO thin films. FIG. 1(B) shows an XRD pattern of the three most intense peaks ((100), (002) and (101), showing shifting of the centre of diffraction toward the left.

This might be due to the lattice disorder and strain induced by interstitial Fe atoms or the substitution of Fe for Zn. The lattice constants of Fe doped ZnO were found to be slightly larger than those of pure bulk ZnO. The larger ionic radii of Fe^{+2} ions (0.63 Å) compared to Zn^{+2} ions (0.60 Å) in the tetrahedral coordination [33] tend to increase the size of the lattice in doped ZnO films. An approximate average size, D, of Fe-ZnO crystal was calculated from the well-known Scherrer formula:

$$D = \frac{K\lambda}{\beta\cos\theta} \tag{7}$$

where; k is a constant equal to 0.9, λ is the incident X-ray wavelength and β is the FWHM in radian. For the pure ZnO sample, the average size D was found to be 70 nm, meanwhile the values of D for all doped samples are listed in Table 1. They obviously increased with doping concentrations. The out-of -plane (along c-axis) strain, ε_c, has been calculated from the relation $\varepsilon_c = \Delta c/c_0$ [34] and presented in Table 1,where; Δc is defined as the deviation of the calculated lattice parameter c from the corresponding unstrained values of bulk ZnO $c_o = 5.206$ Å. The positive values of the out-of-plane strain ε_c indicate that the strain caused by the substrate is tensile in all doped samples.

TABLE 1. Lattice constant (c), out-of -plane strain (ε_c) and average crystal size(D) determined for the Fe-ZnO samples deposited for different durations

Sample	c (Å)	ε_c (%)	D (nm)
0.06 mM Fe	5.216	0.192	31
0.12 mM Fe	5.230	0.461	61
0.18 mM Fe	5.242	0.691	65
0.24 mM Fe	5.242	0.691	86

Fig. 2 shows the scanning electron micrographs of the morphology of ZnO films deposited on gold coated glass substrates using ECD. The films were deposited for different additions of Fe; (0.06, 0.12, 0.18 and 0.24) mM, keeping the current density constant at 3 mA/cm^2 (corresponding to the applied potential voltage of 15 V). The SEM images show different surface morphologies of the grown structures according to the concentration of Fe. As the Fe-concentration increases, changes in the morphology of the films are observed. The surface morphology of the Fe-ZnO thin films shows a network of flake-like nanostructures and clearly revealed that the average size of surface flakes is increased with increasing the concentration of Fe doping, which is in agreement with other results [25]. The flakes are a mixture of small sizes from a micron to100 nm for 0.06 mM Fe (Fig.2b), larger, denser and more uniform flakes with two forms for 0.12 mM Fe (Fig.2c). As the concentration of Fe is increased over 0.18 mM Fe, the flakes become denser and like a continuous structure and the Fe_2O_3 becomes more dominant as shown in (Fig.2d) and (Fig.2e). That is to say, when Fe-doping concentration is less than 0.18 mM Fe, the Fe_2O_3 has little effect on the morphology of ZnO nanostructures. One could observe that the concentration of Fe has a significant effect on the morphology, the shape and the size of the films, such that the dimensions of the structures were observed to increase with increasing the concentration.

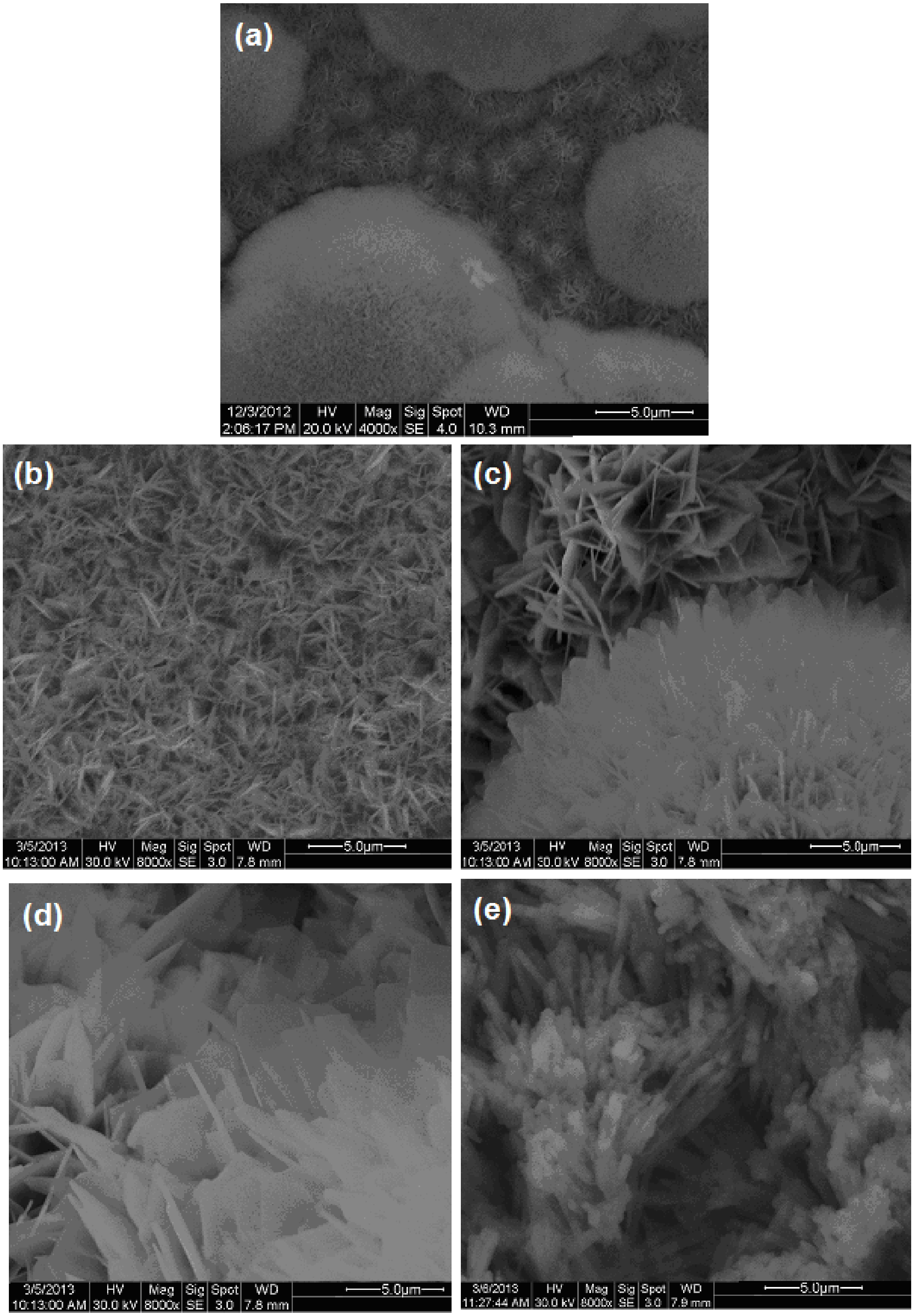

FIG. 2. The surface morphology (SEM) micrographs of (a) pure ZnO, (b) 0.06 mM Fe, (c) 0.12 mM Fe, (d) 0.18 mM Fe and (e) 0.24 mM Fe-doped ZnO thin films

FIG. 3 demonstrates the EDX image of pure and Fe-doped ZnO thin films. The ratios of Fe_2O_3 and ZnO were printed in the figure which shows that the ratio of Fe_2O_3 increased with doping.

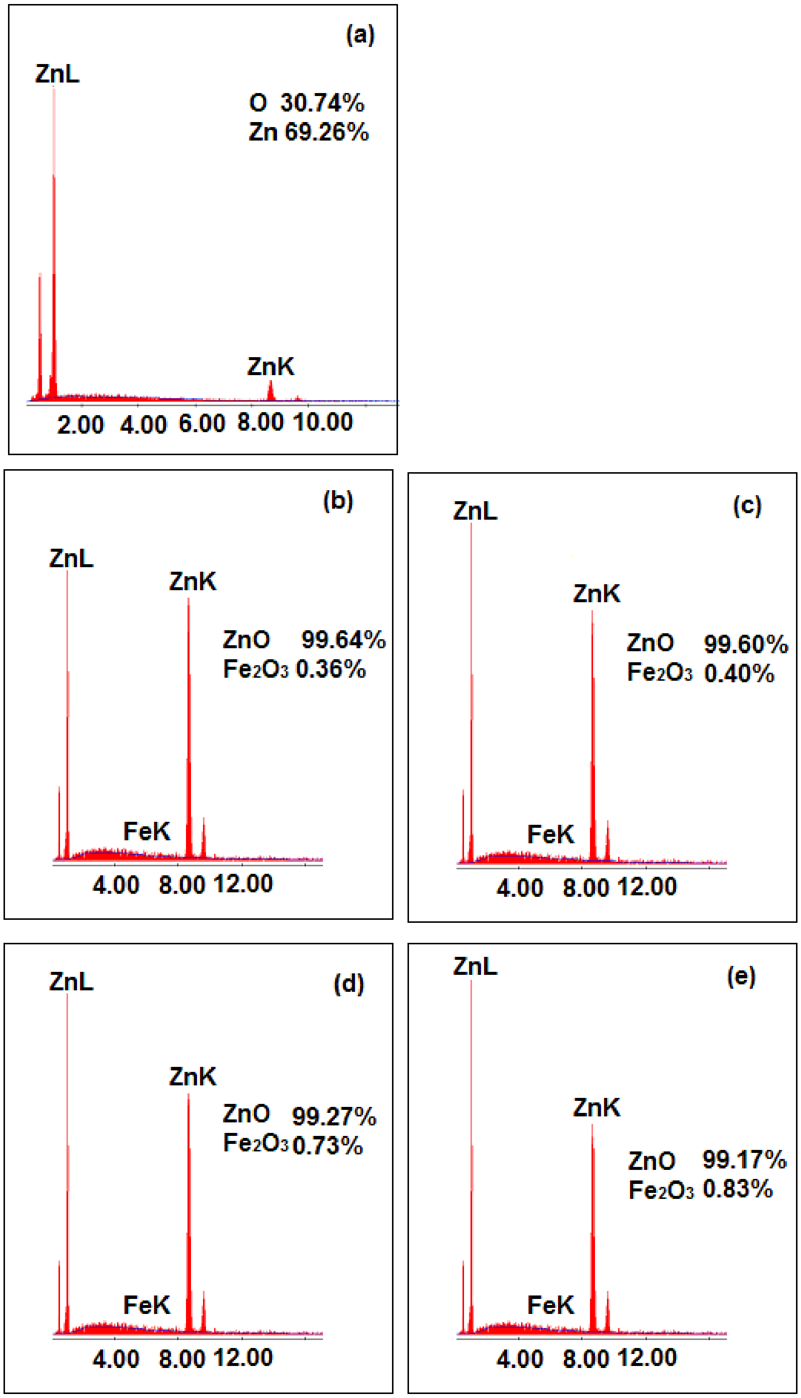

FIG. 3. The EDX spectra of (a) pure ZnO, (b) 0.06 mM Fe, (c) 0.12 mM Fe, (d) 0.18 mM Fe and (e) 0.24 mM Fe-doped ZnO thin films

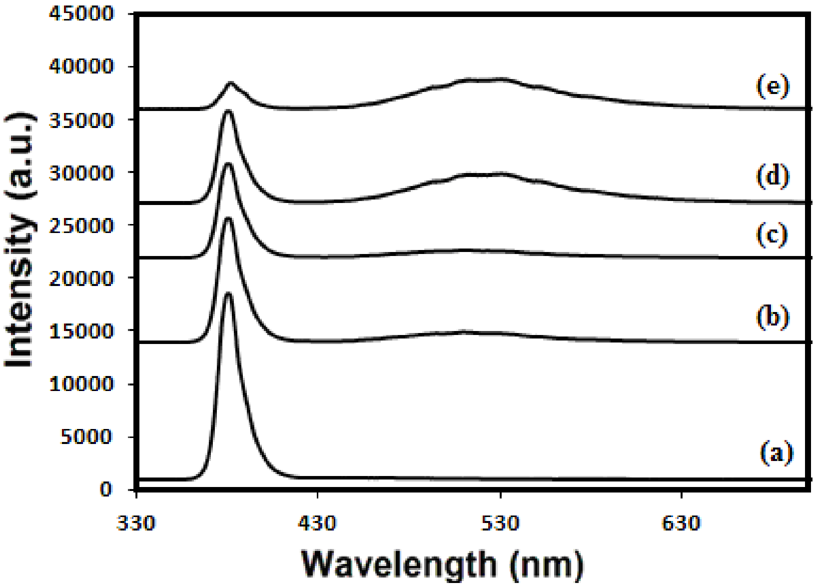

FIG. 4. Room temperature photoluminescence (PL) spectra of (a) pure ZnO, (b) 0.06 mM Fe, (c) 0.12 mM Fe, (d) 0.18 mM Fe and (e) 0.24 mM Fe-doped ZnO thin films

FIG. 4 shows the room-temperature photoluminescence spectra (330-700) nm of pure and Fe-doped ZnO thin films deposited on gold coated glass substrates. All the samples have an ultraviolet emission peak centered at 381 nm and a broad green-orange emission band ranging from (400 - 650) nm. The near band edge emission (NBE) centered at 381 nm is attributed to the irradiative recombination of a hole in the valence band and an electron in the conduction band also from free exciton [35, 36]. Therefore, the density of free exciton in ZnO thin films is the major factor affecting the intensity of ultraviolet emission. This tends to shift the peak continuously toward higher wavelength and broaden the peak with increasing doping concentration. The shift of the NBE emission peak has been attributed to the strong exchange interactions between the ‘d’ electrons of the doping ions, and the ‘s’ and ‘p’ electrons of the host [37]. The green-orange emission band was related to defects; in addition, by increasing the concentration of the doping ions, there is a gradual increase in the intensity of the defect related peak. This indicates that the concentration of intrinsic defects (responsible for broad-band emission) increase with Fe doping in ZnO films. The doped captions may provide competitive pathways for recombination and result in quenching of the broad green-orange emission. It is clear from Fig. 4 that the intensity of ultraviolet emission has obviously decreased while the intensity of the green-orange emission band increased as Fe is added to ZnO thin film.

The above results show that the effect of Fe-doping on the luminescence behavior of ZnO is complex. The complexity is mainly associated with the following factors:

(1) The native point defects (including type and density) in ZnO are different due to the different preparation techniques of ZnO materials.

(2) The valence state of Fe in ZnO is not unique; that is to say, the doped Fe in ZnO may exist either in the form of Fe^{2+} or Fe^{3+} and even coexist in the form of Fe^{2+} and Fe^{3+}.

(3) The inclusion of iron ion which is larger than zinc ion by 6% into the ZnO thin films leads to an increase in the lattice parameter as in table 1 which in turn causes lattice strains by generating intrinsic defects or induces phase separation and/or precipitation of the dopant ions into interacting clusters [38]. This result is clearly manifested by the reduction of luminescence efficiency shown in Figure 4 and the appearance of clustering in SEM micrographs as the concentration of the dopant increases.

FIG. 5 shows the optical transmission spectra of Fe-doped ZnO thin films deposited on gold coated glass substrates at room temperature for different Fe doping concentrations in the corresponding wavelength range of 200-500 nm.

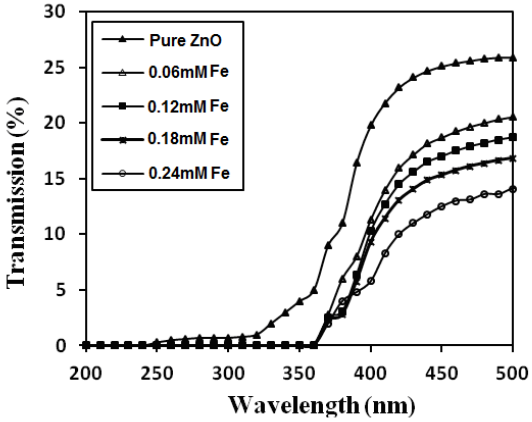

FIG. 5. Transmittance spectra of Fe-doped ZnO thin films.

It is interesting to note that for higher wavelengths (λ > 370 nm), transmission (%) is gradually reduced with Fe doping. The transmittance of Fe-ZnO films in the visible region decreases from 25% to10% as the Fe doping percentage increases. This decrease in the transmittance value of the Fe-ZnO thin films is due to the grain boundary scattering and attributed to the increased scattering of photons by crystal defects created by doping [39]. The free carrier absorption of the photons also contributes to the observed reduction in the optical transmission of heavily doped films. This decrease agrees with other workers. For example, Chen et al. [40] found that the transmittance in the visible region obviously decreased when ZnO thin films were doped with high Fe concentration, which is consistent with our observations. The transmittance curves show that for high energies (lower wavelengths) there is no transmission, because all the light is absorbed. For low energies (higher wavelengths), however, there are no appropriate electronic transitions possible, so the transmission is very high in this range. From transmittance spectra, it is observed that the Fe-ZnO samples show a decrease in the energy band gap from 3.5 eV for pure ZnO to 3.19 eV for Fe-ZnO. A blue shift in the band gap was observed in films as the doping concentration was increased. Band gaps estimated from these spectra were 3.5, 3.3, 3.2, 3.2 and 3.19 eV corresponding to the films deposited at 0.0 mM Fe, 0.06 mM Fe, 0.12 mM Fe, 0.18 mM Fe and 0.24 mM Fe, respectively.

Conclusions

Pure and Fe-ZnO thin films have been successfully synthesized on gold coated glass substrates by low-cost one-step electrodeposition technique. The ZnO film presented a pure phase and a crystal size on the nano-metric scale. From X-ray diffraction analysis, the polycrystalline ZnO with wurtzite structure and the formation of Fe-ZnO composite were also confirmed. Also, the XRD analysis showed that the Fe ions replaced Zn atoms and are incorporated into the crystal lattice positions of ZnO. The surface morphology of the Fe-ZnO thin films shows a network of flake-like nanostructures and clearly revealed that the average size of surface flakes increased with increasing the concentration of Fe doping.

The PL spectra of ZnO films illustrate that the concentration of Fe doping plays an important role in the evolution of PL properties. The intensities of defects emissions increase with the increase of Fe concentration, resulting in the red-shift of emission centre in the PL spectra indicating that more defects were formed in Fe-ZnO doped films. The undoped ZnO thin films exhibited a pure excitonic emission centred at 382 nm, whereas the Fe-ZnO films showed a red shift in UV emission. The transmittance of Fe-ZnO films in the visible region decreases as the Fe doping percentage increases

---

References

[1] Savariumuthu, P.A., Jeong, I.L. and Jin, K.K., Appl. Phys. Lett., 90 (2007) 103.

[2] Saito, N., Haneda, H., Sekiguchi, T., Ohashi, N., Sakaguchi, I. and Koumoto, K., Adv. Mater., 14 (2002) 418.

[3] Ohashi, N., Kataoka, K., Ohgaki, T., Miyagi, T., Haneda, H. and Morinaga, K., Appl. Phys. Lett., 83 (2003) 4857.

[4] Abdulgafour, H.I., Yam, F.K., Hassan, Z., Al-Heuseen, K. and Jawad, M.J., J. Alloys Compd., 509 (2011) 5627.

[5] Choy, J.H., Jang, E.S., Jang, J.H. and Him, Y.W., Adv. Mater., 15 (2003) 1911.

[6] Novotny, I., Sutta, P., Mika F. and Trarozek, V., Proceedings of the International Conference on Microelectronics (IEEE Piscataway, N.J., 1995), p. 65.

[7] Mahnmood, F.S., Gould, R.D., Hassan A.K. and Salih, H.M., Thin Solid Films, 270 (1995) 376.

[8] Bonasewicz, P., Hirschwald, W. and Neumann, G., Thin Solid Films, 142 (1986) 77.

[9] Kuroyanagi, A., Jpn. J. Appl. Phys., 28 (1989) 219.

[10] Gpolaswamy, H. and Reddy, P.J., Semicond. Sci. Technol., 5 (1990) 980.

[11] Gomez, H., Maldonado, A., Asomoza, R., Zironi, E.P., Canetas-Ortega, J. and Palacios-Gomez, J., Thin Solid Films, 293 (1992) 117.

[12] Minami, T., Sato, H., Sohokara, H., Takata, S., Miyata, T. and Fukuda, I., Thin Solid Films, 253 (1994) 14.

[13] Ennaoui, A., Weber, M., Scheer, R. and Lewerenz, H.J., Sol.Energy Mater. Sol. Cells, 54 (1998) 277.

[14] Yingling, Y., Hongwei, Y., Zhengping, F., Beifang, Y., Linsheng, X., Yuandong, X., Jian, Z., Fanqing, L., Solid State Communications, 138 (2006) 521.

[15] Dalchiele, E.A., Giorgi, P., Marotti, R.E., Martin, F., Ramos- Barrado, J.R., Ayouci, R. and Leinen, D., Sol. Energy Mater. and Sol. Cells, 70 (2001) 245.

[16] Fahoume, M., Maghfoul, O., Aggour, M., Hartiti, B., Chralbi, F. and Ennaoui, A., Sol. Energy Mater. and Sol. Cells, 90 (2006) 1437.

[17] Annica, A., Nicklas, J., Per, B., Nu, Y., Donald, L. and Salaneck, W.R., Adv. Mat., 10 (1998) 859.

[18] Sharma, P.K., Dutta, R.K., Pandey, A.C., Layek, S and Verma, H.C., J. Magn. Mater., 321 (2009) 2587.

[19] Pan, F., Song, C., Liu, X.J., Yang, Y.C. and Zeng, F., Mater. Sci. Eng., R 62 (2008) 1.

[20] Van, L.H., Ding, J., Hong, M.H., Fan, Z.C. and Wang, L., Surf. Rev. Lett., 15(2008) 81.

[21] Song, C., Pan, S.N., Liu, X.J., Li, X.W., Zeng, F., Yan, W.S., He, B. and Pan, F., J. Phys.: Condens. Matter, 19 (2007) 176229.

[22] Polyakov, A.Y., Govorkov, A.V., Smirnov, N.B., Pashkova, N.V., Pearton, S.J., Ip, K., Frazier, R.M., Abernathy, C.R., Norton, D.P., Zavada, J.M. and Wilson, R.G., Mater. Sci. Semicond. Process, 7 (2004) 77.

[23] Janisch, R., Gopal, P. and Spaldin, N.A., J. Phys.: Condens. Matter, 17 (2005) R657.

[24] Debernardi, A. and Fanciulli, M., Appl. Phys. Lett., 90 (2007) 212510.

[25] Sato, K. and Katayama-Yoshida, H., Physica E, 10 (2001) 251.

[26] Wei, X.X., Song, C., Geng, K.W., Zeng, F., He, B. and Pan, F.J. Phys: Condens. Matter, 18 (2006) 7471.

[27] Karmakar, D., Mandal, S.K., Kadam, R.M., Paulose, P.L., Rajarajan, A.K., Nath, T.K., Das, A.K., Dasgupta, I. and Das, G.P., Phys. Rev. B, 75(2007) 144404.

[28] Feng, Q.J., Shen, D.Z., Zhang, J.Y., Li, B.H., Zhang, Z.Z., Lu, Y.M. and Fan., X.W., Mater. Chem. Phys., 112 (2008) 1106.

[29] Ishizaki, H., Imaizumi, M., Matsuda, S., Izaki, M. and Ito, T., Thin Solid Films, 411 (2002) 65.

[30] Hosik, P., Perla, A., Marc, A. D., Ashok, M., Heechul, C. and Nosang V. Myung. Chemical Engineering Journal, 139 (2008) 208.

[31] Chen, Z.C., Zhug, L.J., Wu, X.M. and Meng, Y.D., Thin Solid Films, 515 (2007) 5462.

[32] Panigrahy, B., Aslam, M. and Bahadur, D., J. Phys. Chem., C114 (2010) 11758.

[33] Barick, K.C., Aslam, M., Dravid, V.P. and Bahadur. D., J. Phys. Chem., C112 (2008) 15163.

[34] Krüger, J., Sudhir, G.S., Corlatan, D., Cho, Y., Kim, Y., Klockenbrink, R., Rouvimov, S., Liliental-Weber, Z., Kisielowski, C., Rubin, M. and Weber E.R., Mater. Res. Symp. Proc. 482 (1998).

[35] Wu, J.J., Wen, H.I., Tseng, C.H. and Liu, S.C., Adv. Funct. Mater., 14 (2004) 806.

[36] Chang, Y.C. and Chen, L.J., J. Phys. Chem., C111 (2007)1268.

[37] Panigrahy, B., Aslam, M. and Bahadur, D., J. Phys. Chem., C114 (2010)11758.

[38] Wang, Y., Milosevic, O., Gomez, L., Rabanal, M.E., Torralba, J.M., Yang, B. and Townsend, P.D., J. Phys. Condens. Matter, 18 (2206) 9257.

[39] Joseph, B., Manoj, P.K. and Vaidyan, V.K., Ceram. Int., 32 (2006) 487.

[40] Chen, Z.C., Zhuge, L.J., Wu, X.M. and Meng, Y.D., Thin Solid Films, 515 (2007) 5462.